SUPPORTING INFORMARION

High Brightness Circularly Polarized Blue Emission from Non-doped OLEDs Based on Chiral Binaphthyl-Pyrene Emitters

Xueyan Zhang,[a] Yu Zhang,[a] Yang Li,[a] Yiwu Quan,*[a] Yixiang Cheng*[b], and Yunzhi Li, *[c]

a. Key Laboratory of High Performance Polymer Materials & Technology of Ministry of Education, School of Chemistry and Chemical Engineering, Nanjing University, Nanjing 210023, China. E-mail: quanyiwu@nju.edu.cn

b. Key Lab of Mesoscopic Chemistry of MOE and Jiangsu Key Laboratory of Advanced Organic Materials, School of Chemistry and Chemical Engineering, Nanjing University, Nanjing 210023, China. E-mail: yxcheng@nju.edu.cn.

c. School of Chemistry and Chemical Engineering, Linyi University, Linyi, 276000, China. E-mail: liyunzhi@lyu.edu.cn.

Contents

1. Experimental section S2

2. Thermal Properties of Compounds *S*-5 and *S*-6 ..... S4

3. Photophysical Properties of Compounds *R*-/*S*-*5* and *R*-/*S*-*6* S4

4. Electrochemical Measurements S7

5. Theoretical calculations S8

6. Electroluminescence Spectra of Devices based on *R*-/*S*-5 and *R*-/*S*-6 ..... S10

7. NMR Spectra *vs* HRMS Spectra of Compounds S12

1. Experimental section

General Methods.

All reagents were commercial analytical reagents (A.R.), which were used directly without further purification. The solvent THF was distilled from sodium and benzophenone, and freshly distilled prior to use.

All NMR spectra were measured on a Bruker 400 MHz spectrometer. Thermogravimetric analysis (TGA) was performed on a Pyris 1 TGA Perkin Elmer thermogravimetric analyzer under a N_2 atmosphere with a heating rate of 10 °C min^{-1} from 25°C to 700 °C. Differential scanning calorimetry (DSC) was performed with a Q2000 DSC differential scanning calorimeter under a N_2 atmosphere with a heating rate of 10 °C min^{-1} from 25°C to 250 °C. HRMS were measured on an FTMS instrument. Cyclic voltammetry (CV) was performed on a CHI-600C electrochemical analyzer. The CV measurements were carried out with a conventional three-electrode configuration consisting of a glassy carbon working electrode, a platinum-disk auxiliary electrode and an $Ag/AgNO_3$ reference electrode, and the scan speed was 100 mV s^{-1}. UV-*vis* absorption spectra were obtained by using a Hitashi U-3900 absorption spectrophotometer. Fluorescence spectra were measured by using a HORIBA Scientific Fluoro-max-4 Spectrofluorometer at 298 K. The fluorescent quantum yield was measured by using integrating sphere method. Circular dichroism (CD) spectra were obtained on a JASCO *J*-810 spectropolarimeter. Circularly polarized luminescence (CPL) spectra were recorded by a JASCO CPL-300 spectrofluoropolarimeter. All measurements were performed at room temperature unless otherwise stated.

Device Fabrication and Characterization.

The proof-of-concept OLEDs were fabricated by using the solution processing methods. The ITO glass substrates (1.5 cm × 1.5 cm) were washed by CH_2Cl_2, acetone, ultrapure water and ethanol in order; dried in an oven at 120 °C for about 0.5 h; and treated with UV-ozone for 15 min. Then, the substrates were transferred to a glove box to spin-coated PEDOT:PSS layer. Emitting organic layers were spin-coated on the substrate that were pre-coated with ITO and PEDOT:PSS layers by solution-processing. 1,3,5-tri(1-phenyl-1H-benzo[*d*]imidazol-2-yl)phenyl (TPBI) was served as electron-transporting layer (ETL), Ca/Ag were evaporated as cathode, TPBI and cathode materials were fabricated by high-vacuum (1×10^{-5} Pa and 5×10^{-4} Pa, respectively.) thermal evaporation onto device films in sequence. TPBI, Ca and Ag were deposited at rates of 0.5, 0.5 and 1 Hz s^{-1}, respectively. The electroluminescent spectra were recorded on a Hitachi MPF-4 fluorescence spectrometer. The current density-voltage-luminance (*J-V-L*) and current efficiency-luminance (*CE-L*) characteristics of OLEDs were recorded on a Keithley 2636A Source meter coupled with Si-photodiodes calibrated with Photo-Research PR-655. The EL spectra were measured by using a Photo Research PR-655 Spectra Scan. The devices without any encapsulation and all measurements were carried out under ambient atmosphere.

Synthesis Procedures

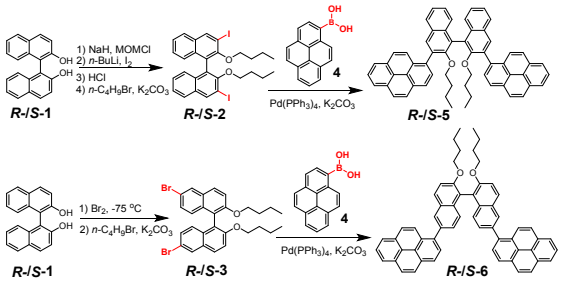

Scheme 1 The synthesis procedures of ***R***-/***S***-**5** and ***R***-/***S***-**6.**

Compounds *R*-/*S*-2 were synthesized according to the literature[1] to afford **2** as two pale yellow solids (48% yield). ***R*-2**: ^{1}H NMR (400 MHz, $CDCl_3$) δ (ppm): 8.51 (s, 2H), 7.79-7.72 (d, J = 8.4 Hz, 2H), 7.41-7.35 (m, 2H), 7.24-7.20 (m, 2H), 7.12-7.10 (d, J = 8.4 Hz, 2H), 3.84-3.79 (m, 2H), 3.32-3.28 (m, 2H), 1.32-1.16 (m, 4H), 0.95-0.90 (m, 2H), 0.77-0.73 (m, 2H), 0.58-0.46 (m, 6H).

Compounds *R*-/*S*-3 were synthesized according to the literature[2] to afford **3** as two white solids (94% yield). ***R*-3**: ^{1}H NMR (400 MHz, $CDCl_3$) δ (ppm): 8.51 (s, 2H), 7.80-7.70 (d, J = 8.4 Hz, 2H), 7.45-7.36 (m, 2H), 7.24-7.18 (m, 2H), 7.15-7.10 (d, J = 8.4 Hz, 2H), 4.20-4.05 (m, 4H), 1.60-1.50 (m, 4H), 1.20-1.06 (m, 4H), 0.80-0.70 (t, J = 7.7 Hz, 6H).

Syntheses of *R*-/*S*-5. A 50mL Schlenk tube was charged with intermediate ***R*-2** (0.32 g, 0.49 mmol), compound **4** (0.27g, 1.07 mmol), $Pd(PPh_3)_4$ (0.023 g, 0.02 mmol), anhydrous K_2CO_3 (0.68 g, 5 mmol), tetrabutyl ammonium bromide (0.064 g, 0.2 mmol), toluene (15 mL), distilled water (2 ml). The reaction mixture was heated at 90 °C for 24 h. After cooling down to room temperature, the mixture was subsequently diluted with dichloromethane (50 mL), washed with water (30 mL) and dried over $NaSO_4$. After removing the solvents under reduced pressure, the residue was purified by silica gel column chromatography (petroleum ether / ethyl acetate = 50/1, v/v) to afford a white solid. ***R*-5**: 58% yield. ^{1}H NMR (400 MHz, DMSO-d_6) δ (ppm): 8.70-8.0 (m, 22H), 7.71-7.40 (m, 6H), 3.40-3.10 (m, 4H), 1.10-0.90 (m, 1H), 0.88-0.39 (m, 9H), 0.20-0.05 (m, 4H). ^{13}C NMR (100 MHz, $CDCl_3$) δ (ppm): 154.53, 135.44, 134.79, 133.98, 132.20, 131.23, 130.42, 129.45, 128.32, 127.67, 126.21, 124.92, 72.82, 67.15, 31.55, 18.29, 12.95. HRMS (ESI$^+$): m/z $[M + Na]^+$ calcd for $[C_{60}H_{46}O_2\ Na]^+$: 821.3390; found: 821.3371. $[\alpha]_D^{25}$ = +29 (c =0.1, in THF). ***S*-5**: 63% yield. ^{1}H NMR (400 MHz, $CDCl_3$) δ (ppm): 8.40-7.90 (m, 22H), 7.61-7.35 (m, 6H), 3.40-3.05 (m, 4H), 1.0-0.82 (m, 1H), 0.80-0.25 (m, 9H), 0.20-0.04 (m, 4H). HRMS (ESI$^+$): m/z $[M + Na]^+$ calcd for $[C_{60}H_{46}O_2\ Na]^+$: 821.3390; found: 821.3377. $[\alpha]_D^{25}$ = -30 (c =0.1, in THF).

Syntheses of *R*-/*S*-6. Compound ***R*-/*S*-6** were synthesized according to the procedure of ***R*-5** to afford ***R*-/*S*-6** as white solids. ***R*-6** (yield: 59 %): ^{1}H NMR (400 MHz, $CDCl_3$) δ (ppm): 8.40-7.95 (m, 22H), 7.61-7.40 (m, 6H), 4.20-4.05 (m, 4H), 1.60-1.45 (m, 4H), 1.20-1.06 (m, 4H), 0.80-0.70 (t, J = 7.7 Hz, 6H). ^{13}C NMR (100 MHz, $CDCl_3$) δ (ppm): 154.85, 138.19, 136.25, 133.66, 131.72, 130.74, 129.29, 128.16, 126.05, 125.08, 120.71, 116.18, 69.42, 31.72, 19.09, 13.92. HRMS (ESI$^+$): m/z $[M + H]^+$ calcd for $[C_{60}H_{47}O_2]^+$: 799.3571; found: 799.3573. $[\alpha]_D^{25}$ = +148 (c =0.1, in THF). ***S*-6**: 61% yield. ^{1}H NMR (400 MHz, $CDCl_3$) δ (ppm): 8.40-7.90 (m, 22H), 7.61-7.40 (m, 6H), 4.20-4.05 (m, 4H), 1.60-1.45 (m, 4H), 1.20-1.09 (m, 4H), 0.82-0.68 (t, J = 7.7 Hz, 6H). HRMS (ESI$^+$): m/z $[M + H]^+$ calcd for $[C_{60}H_{47}O_2]^+$: 799.3571; found: 799.3579. $[\alpha]_D^{25}$ = -147 (c =0.1, in THF).

2. Thermal Properties of Compounds *S*-5 and *S*-6

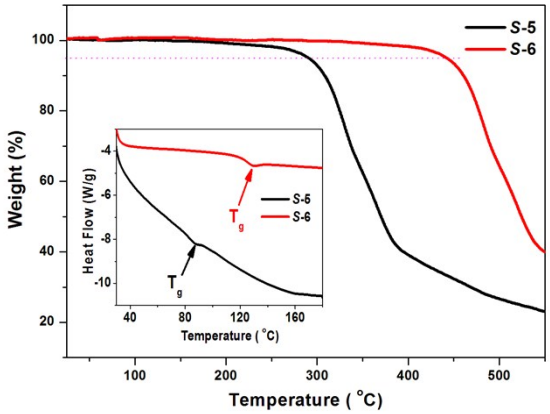

Fig S1. TGA curves of ***S*-5** and ***S*-6**; Inset curve: DSC curves of ***S*-5** and ***S*-6**

3. Photophysical Properties of Compounds *R*-/*S*-*5* and *R*-/*S*-*6*

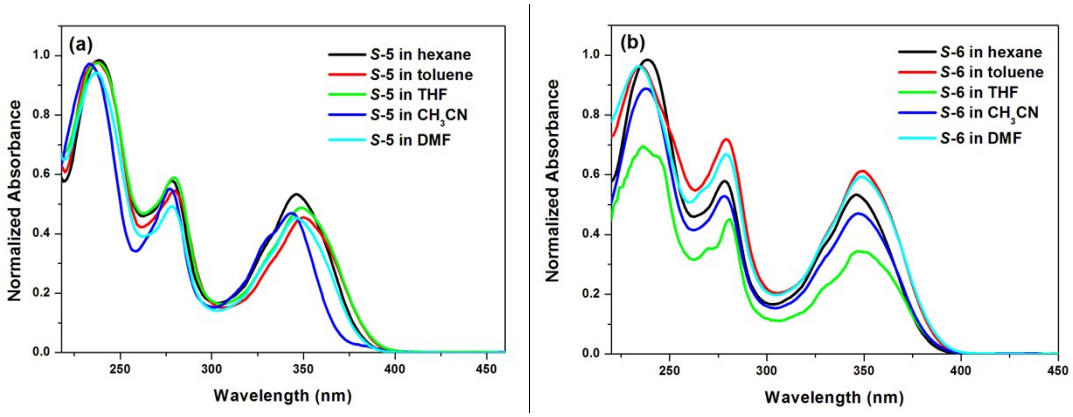

Fig S2. UV-*vis* absorption spectra of ***S*-5** and ***S*-6** in different solvents (1.0×10^{-5} M)

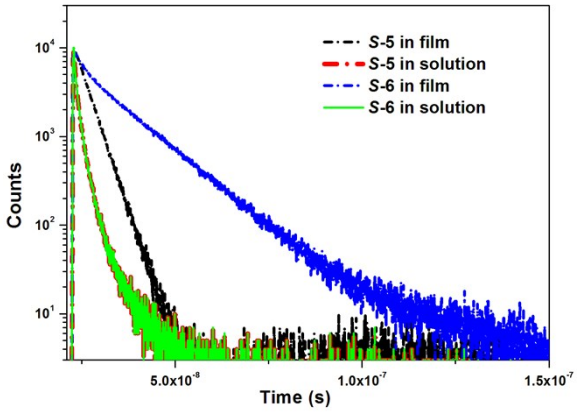

Fig S3. Lifetimes of ***S*-5** and ***S*-6** in spin-coated film and THF solution (1.0×10^{-5} M)

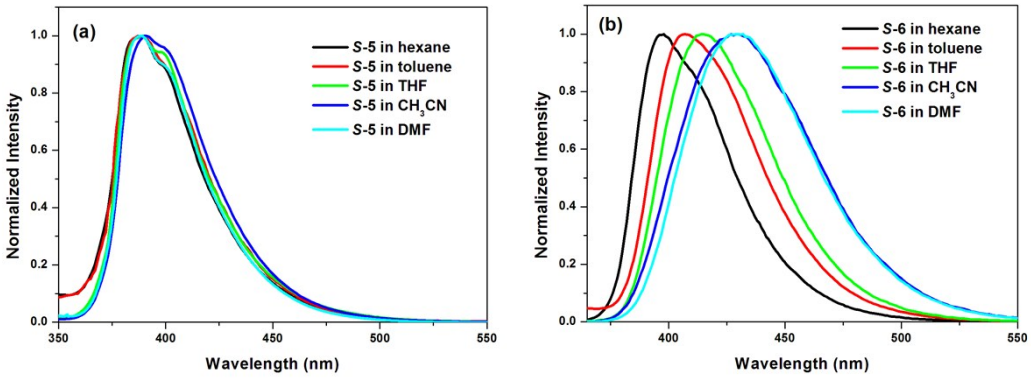

Fig S4. Fluorescence spectra of ***S*-5** and ***S*-6** in different solvents (1.0×10^{-5} M; λ_{ex} = 280 nm)

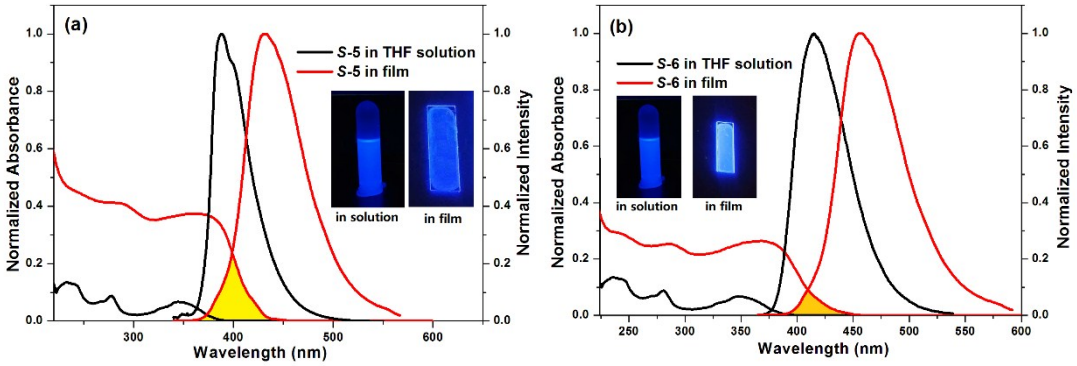

Fig S5 UV-*vis* absorption and fluorescence emission spectra in THF solution (1×10^{-5} M; λ_{ex} = 280 nm) and spin-coated film of ***S*-5** (a) and ***S*-6** (b) (the self-absorption of emitters as shown in highlighted spectral overlap); inset color images: photograph of ***S*-5** and ***S*-6** in THF solution and neat film under UV illumination (365 nm).

Table S1 Optical properties of compounds ***S*-5** and ***S*-6**

Compounds	λ_{abs} / nm		λ_{em}/ nm		Φ_F (%) [c]		T_d (℃)	T_g (℃)
	Soln[a]	Film[b]	Soln[a]	Film[b]	Soln	Film		
***S*-5**	237, 278, 350	284, 362	389	431	80	45.7	284	89
***S*-6**	236, 279, 350	285, 368	416	456	92	56.4	434	136

a: In THF solution (1×10^{-5} M). b: Film spin-coated on quartz plate.

c: Quantum yield of the solutions and films were measured by an integrating sphere.

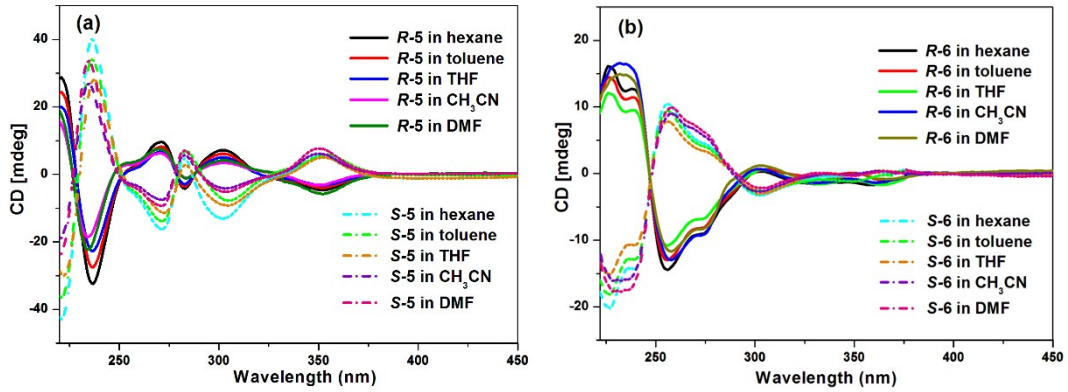

Fig S6 CD spectra of ***R***-/***S***-**5** and ***R***-/***S***-**6** in different solvents (1.0×10^{-5} M).

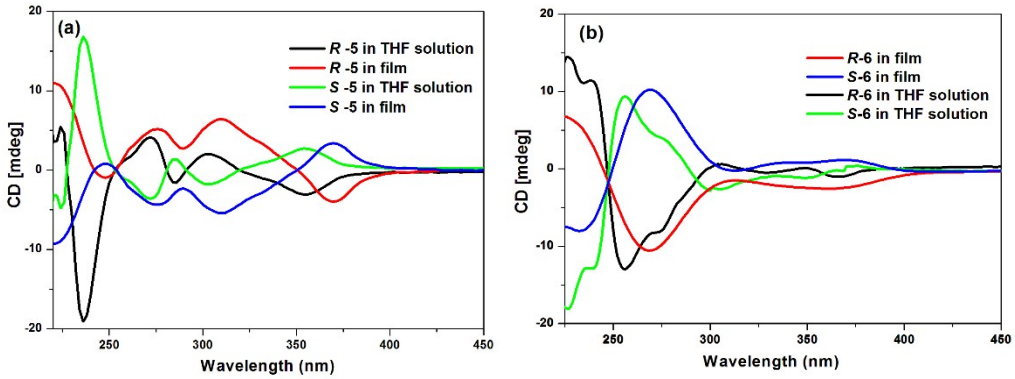

Fig S7 CD spectra of ***R***-/***S***-**5** and ***R***-/***S***-**6** in THF solution (1×10^{-5} M) and spin-coated film.

Flipping ECD spectra for enantiomers *R*-/*S*-5 and *R*-/*S*-6

To better understand the contributions from the isotropic circular dichroism (CD_{iso}) and the linear dichroism/linear birefringence (LDLB) effects on ECD spectra, we examined the ECD spectra of enantiomers ***R***-/***S***-**5** and ***R***-/***S***-**6** in thin films upon sample flipping (front side or back side: switching the face of the detection sample films ‘‘back’’ or ‘‘front’’ toward the incident light.). These thin films were prepared as follow: (1) drop casting films DC-***R***-/***S***-**5** and DC-***R***-/***S***-**6** were obtained by depositing on a quartz plate about 100 μL of 1 mg/mL solutions in THF and then followed by slow evaporation of the solvent in an atmosphere saturated with THF vapours; (2) spin casting films SC-***R***-/***S***-**5** and SC-***R***-/***S***-**6** were prepared by depositing on a quartz plate 100 μL of 10 mg/mL solutions in THF with angular speed of 3000 rpm. [6] All of these films were not further carried out by thermal annealing procedure.

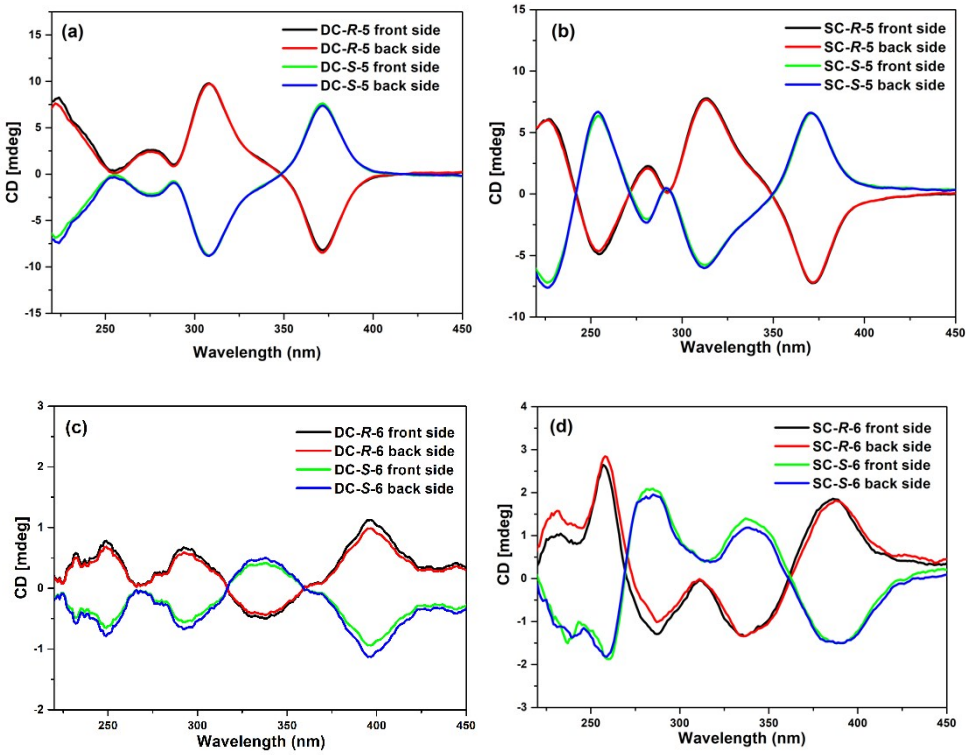

Fig S8 ECD spectra for the front side and back side of enantiomers ***R***-/***S***-**5** and ***R***-/***S***-**6**.

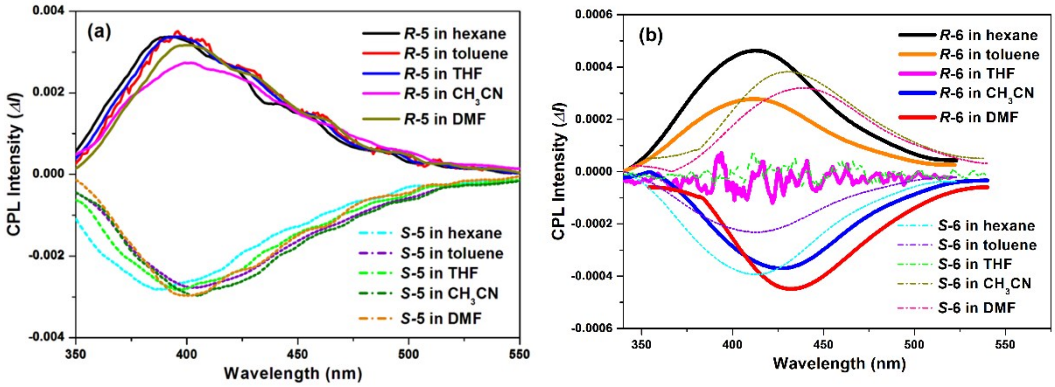

Fig S9 CPL spectra of ***R***-/***S***-**5** and ***R***-/***S***-**6** in different solvents (1.0×10^{-5} M; λ_{ex} = 280 nm).

4. Electrochemical Measurements

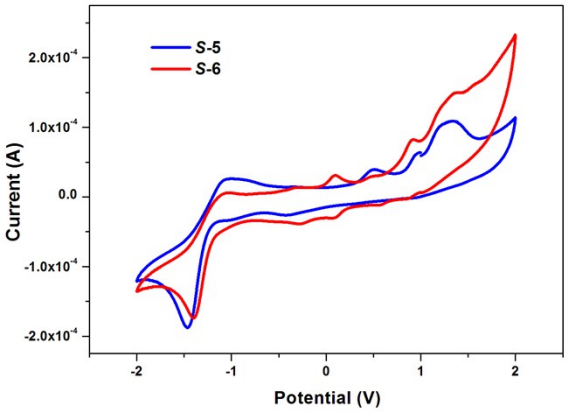

Fig S10 CV curves of ***S*-5** and ***S*-6** in CH_3CN solution

5. Theoretical calculations

To better understand the unique CPL behaviors of ***R*-/*S*-5** and ***R*-/*S*-6**, a series of *ab initio* calculations were performed for ***S*-5** and ***S*-6**. In this study, all ground-state geometries (S_0) were optimized at the B3LYP-D3(BJ)/6-31G** level. Based on the optimized S_0 structures, the relative energy required for the dihedral angle change of the BINOL moiety, and the corresponding first excited-state (S_1) structures were then optimized at the same theory level as described above. Finally, the dissymmetry factor g_{em} values were calculated by the equation $g_{em} = 4RS/DS$, where the *RS* is the rotational strength and the *DS* is the dipole strength at the S_1 state. [3, 4] In this work, all calculations were performed with the Gaussian 09 package.[5]

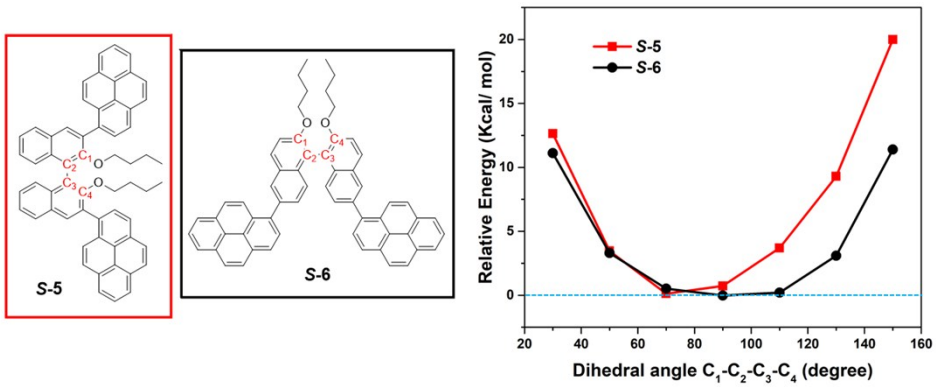

Fig S11 Relative energy required for the dihedral angle change of the BINOL moiety.

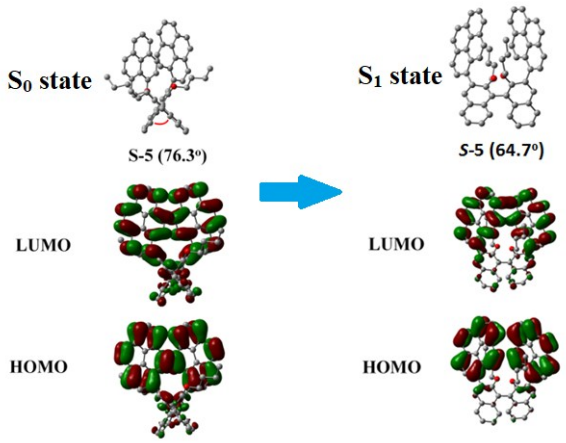

Fig S12 The S_0 and S_1 state structures for ***S*-5**. For clarity, the corresponding H atoms have been omitted.

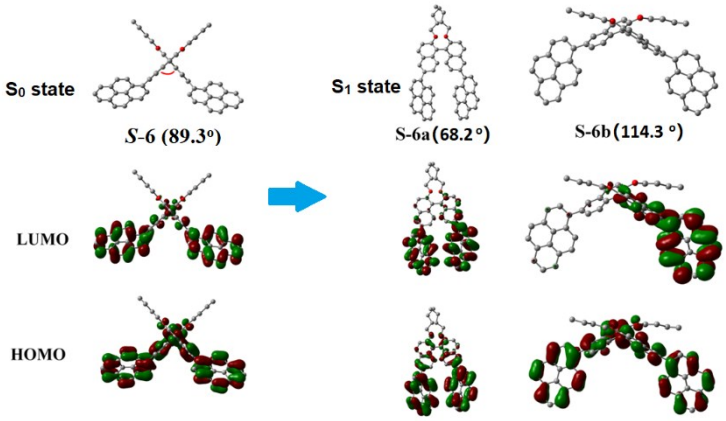

Fig S13 The S_0 and S_1 state structures for ***S*-6** (conformers ***S*-6a** and ***S*-6b**). For clarity, the corresponding H atoms have been omitted.

Table S2 Electrochemical characteristic properties of compounds ***S*-5** and ***S*-6**

Compounds	[a]$\lambda_{abs,\ onset}$ (nm)	[a]E_g (eV)	$E_{ox,onset}$ (V)	[a]HOMO/LUMO (eV)	[b]$\lambda_{abs,\ onset}$ (nm)	[b]HOMO/LUMO (eV)	[b]E_g (eV)
***S*-5**	391	3.17	0.51	-5.11 /-1.94	394	-5.18 /-1.54	3.64
***S*-6**	394	3.15	0.1	-4.70 /-1.55	398	-5.04 /-1.52	3.52

a: Measured in CH_3CN at room temperature in the presence of ***S*-5** or ***S*-6** (0.5 mmol/L), ferrocene (0.5 mmol/L) as an internal standard, and *n*-Bu_4NPF_6 (0.1 M) as an electrolyte; $E_g = 1240/\lambda_{onset,}$ calculated from the absorption edge; $E_{HOMO} = -(E_{ox,\ onset} - E(Fc/Fc^+) + 4.8)$ eV, $E(Fc/Fc^+) = 0.20$ V vs $Ag/AgNO_3$; $E_{LUMO} = E_{HOMO} + E_g$; b: Values in parentheses are obtained at the B3LYP-D3(BJ)/6-31G** level.

Table S3. The calculated emission energies, oscillator strengths, and g_{em} properties from the optimized S_1 geometries.

Compounds	dihedral angle (S_0)	dihedral angle (S_1)	Emission energies (nm)	$^a\lambda_{em}$ (nm)	$^ag_{em}$ (10^{-3})	Oscillator strengths	*DS* (10^{-40} cgs)	*RS* (10^{-40} cgs)	g_{em} (10^{-3})
***S*-5**	76.3 º	64.7º	473.8	389	-2.9	0.08	78441.68	-18.87	-1.0
***S*-6a**	89.3º	68.2º	451.4	416	---	0.01	13702.23	-9.58	-2.8
***S*-6b**	89.3º	114.3 º	448.5	416	---	0.01	11101.52	4.3231	+1.6

a: Measured in THF solution at room temperature in the presence of ***S*-5** or ***S*-6** (1.0×10^{-5} M).

6. Electroluminescence Spectra of Devices based on *R*-/*S*-5 and *R*-/*S*-6

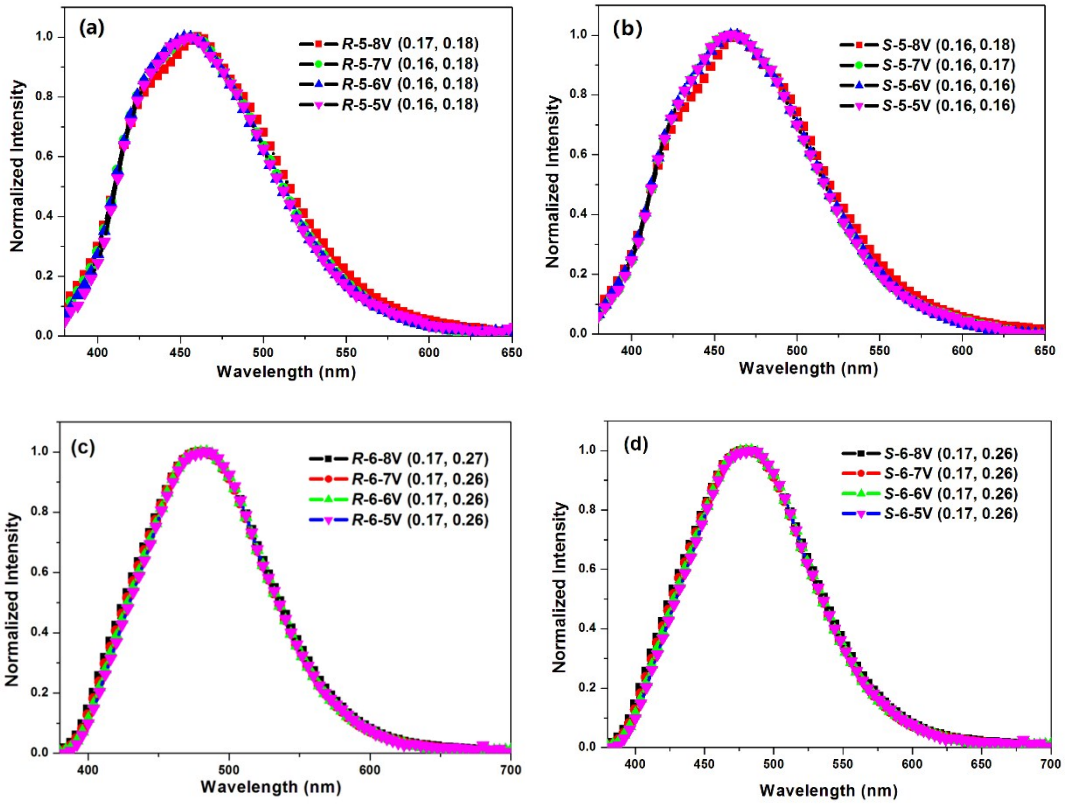

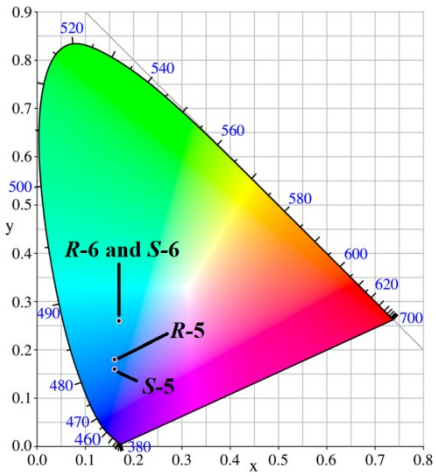

Fig S14 Electroluminescence spectra and corresponding CIE diagram of devices (Ag = 100 nm) based on ***R***-/***S***-**5** and ***R***-/***S***-**6**.

Table S4 Electroluminescence characteristic performance for devices (Ag = 100 nm) based on ***R***-/***S***-**5** and ***R***-/***S***-**6**.

EML (35nm)	[a] CIE (x, y)	[b] V_{on} (V)	[c] CE_{max} (cd A^{-1})	[d] L_{max} (cd m^{-2})	[e] EQE_{max} (%)	[f] g_{EL}
***R*-5**	0.16, 0.18	3.18	3.91	11336	2.79	$+5.6\times10^{-3}$
***S*-5**	0.16, 0.16	3.43	3.86	10886	2.17	-5.2×10^{-3}
***R*-6**	0.17, 0.26	3.18	5.17	24806	3.09	$+7.8\times10^{-4}$
***S*-6**	0.17, 0.26	3.18	4.26	22880	2.27	-7.4×10^{-4}

[a] CIE coordinates of driving voltages at 6 V; [b] Turn-on voltage; [c] Maximum Luminous e□ciency; [d] Maximum luminance; [e] Maximum EQE; [f] Electroluminescence dissymmetry factors of driving voltages at 6 V.

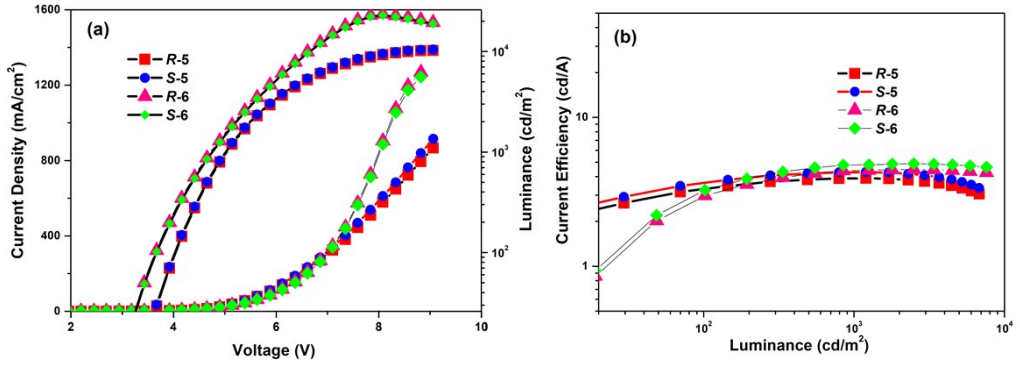

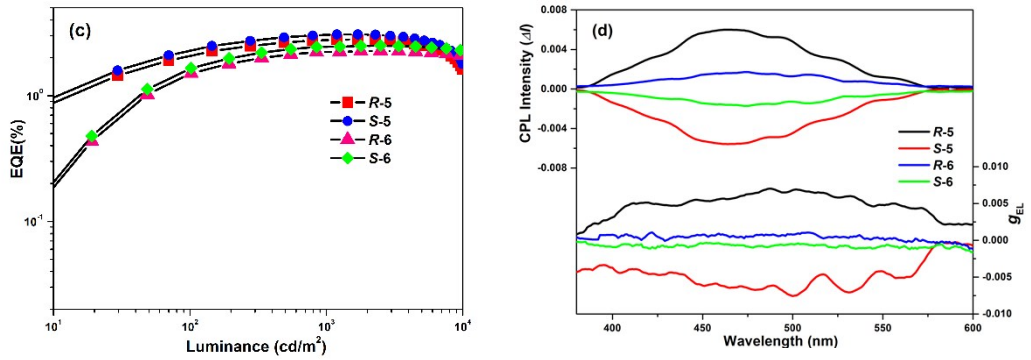

Fig S15 Electroluminescence performance for devices (Ag = 50 nm): (a) the current density-voltage-luminance curves; (b) current efficiency-luminance curves; (c) EQE spectra devices based on ***R***-/***S***-**5** and ***R***-/***S***-**6**; (d) CP-EL spectra of CP-OLEDs based on emitters ***R***-/***S***-**5** and ***R***-/***S***-**6**.

Table S5 Electroluminescence characteristic performance for devices (Ag = 50 nm) based on ***R***-/***S***-**5** and ***R***-/***S***-**6**.

EML (35nm)	[a] CIE (x, y)	[b] V_{on} (V)	[c] CE_{max} (cd A^{-1})	[d] L_{max} (cd m^{-2})	[e] EQE_{max} (%)	[f] g_{EL}
R-**5**	0.16, 0.17	3.18	3.89	10244	2.81	$+5.4\times10^{-3}$
S-**5**	0.16, 0.17	3.18	4.28	10448	3.07	-6.2×10^{-3}
R-**6**	0.18, 0.26	2.8	4.48	23600	2.27	$+7.5\times10^{-4}$
S-**6**	0.18, 0.26	2.8	4.89	22800	2.50	-8.3×10^{-4}

7. NMR Spectra *vs* HRMS Spectra of Compounds

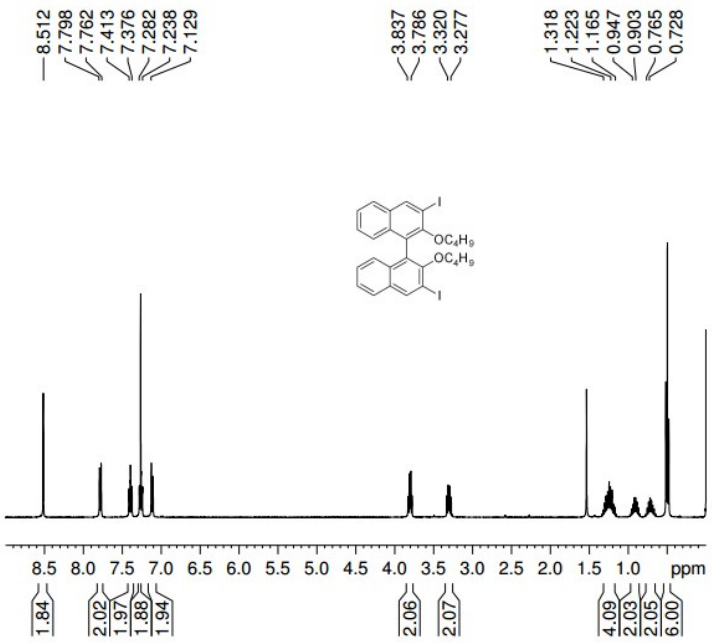

^{1}H NMR spectra of compound ***R*-2**

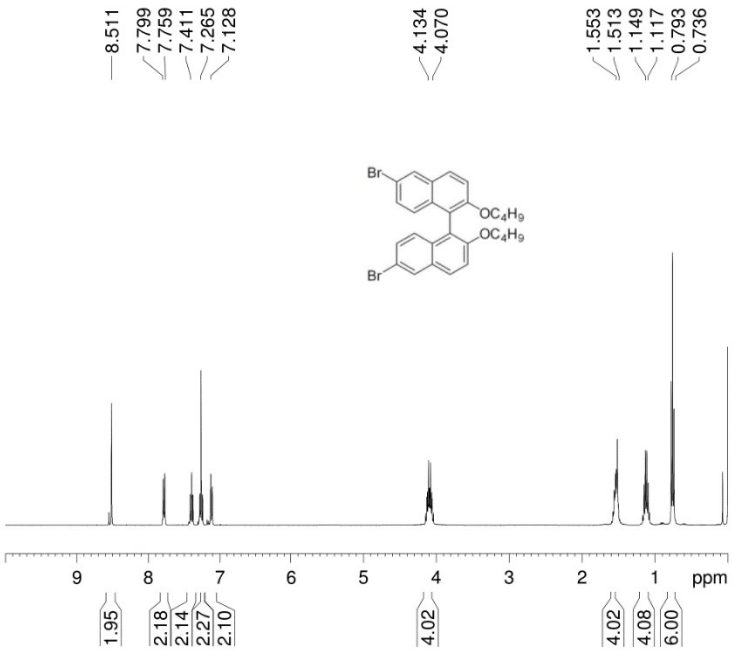

^{1}H NMR spectra of compound ***R*-3**

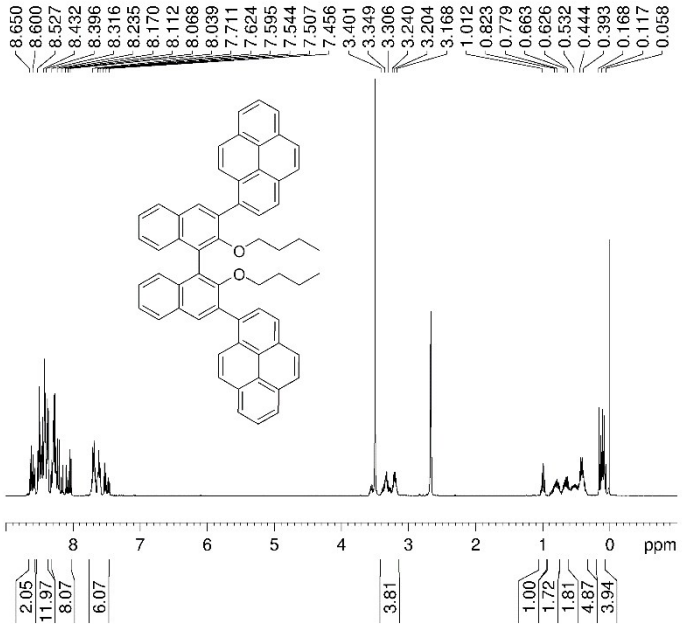

^{1}H NMR spectra of compound ***R*-5**

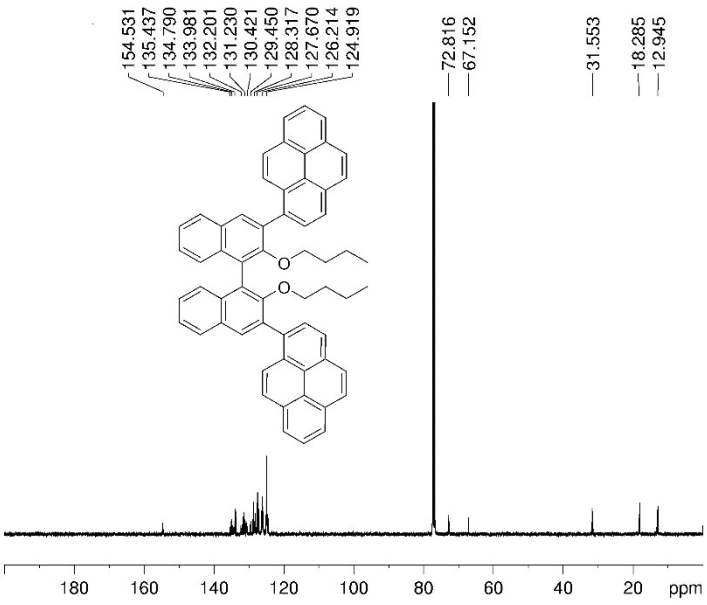

^{13}C NMR spectra of compound ***R*-5**

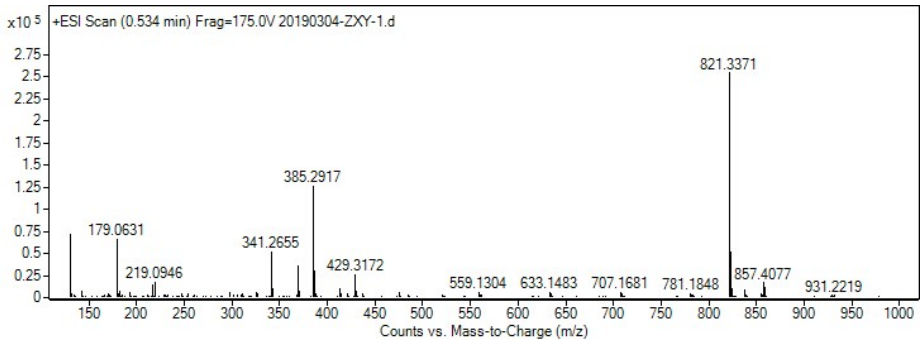

HRMS spectra of compound ***R*-5**

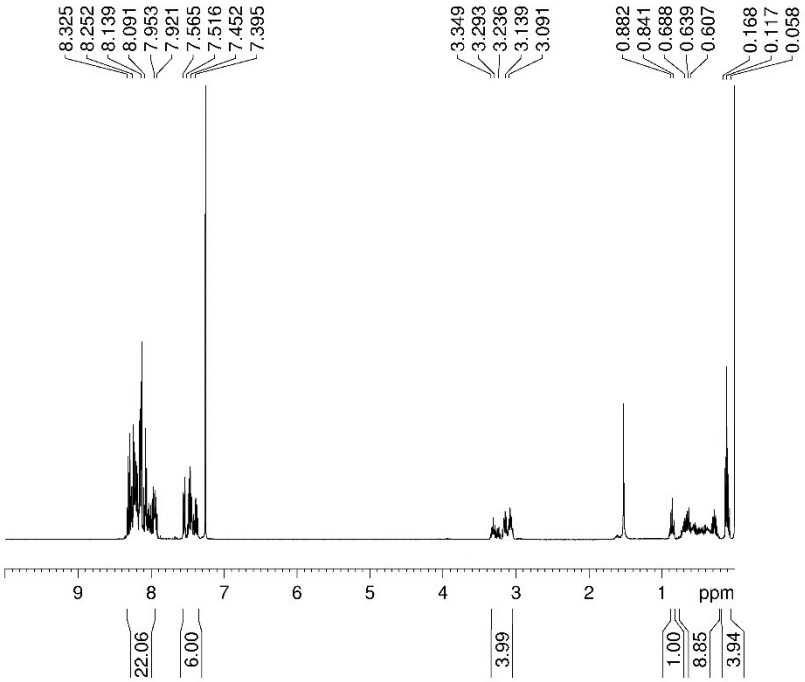

^{1}H NMR spectra of compound ***S*-5**

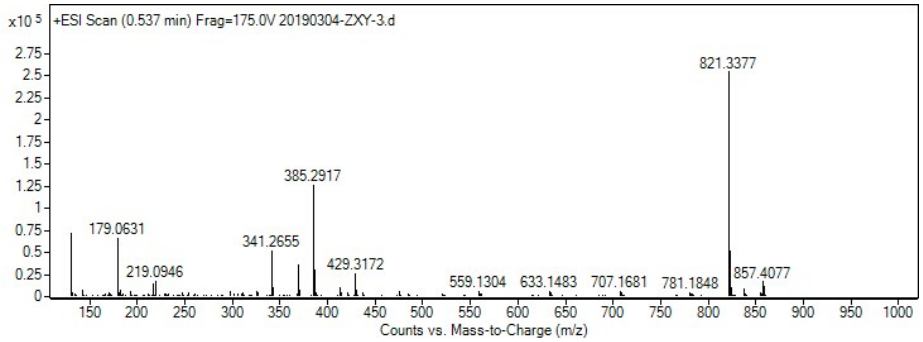

HRMS spectra of compound ***S*-5**

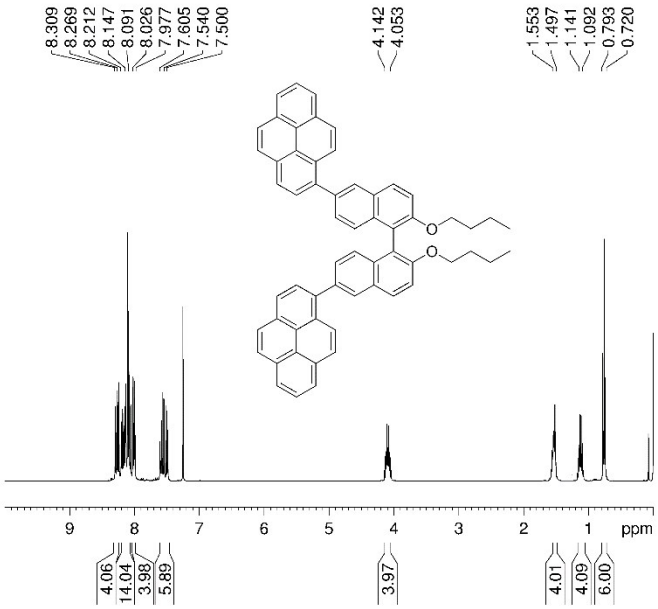

^{1}H NMR spectra of compound ***R*-6**

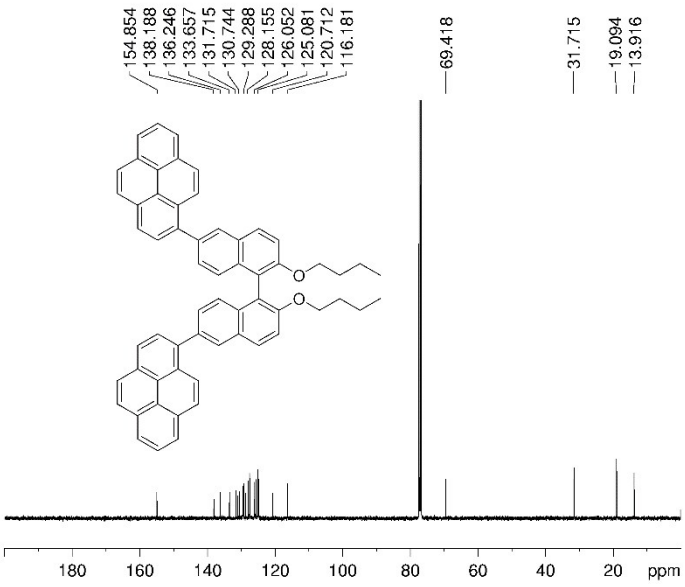

^{13}C NMR spectra of compound ***R*-6**

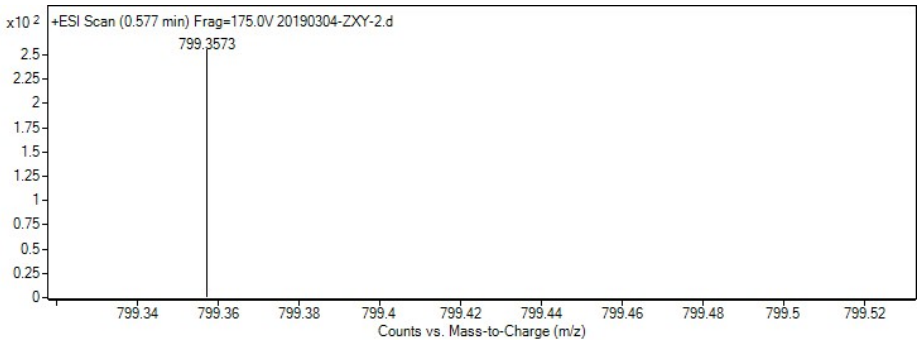

HRMS spectra of compound ***R*-6**

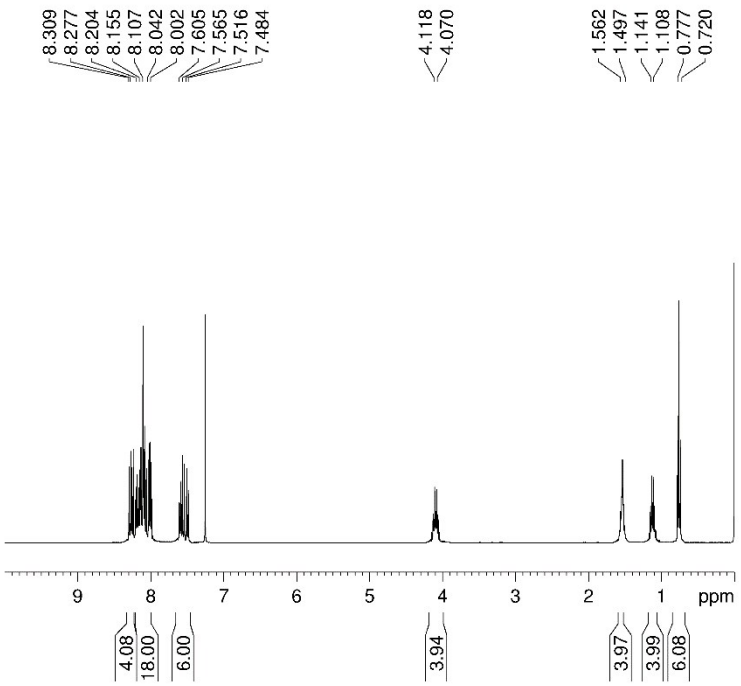

^{1}H NMR spectra of compound ***S*-6**

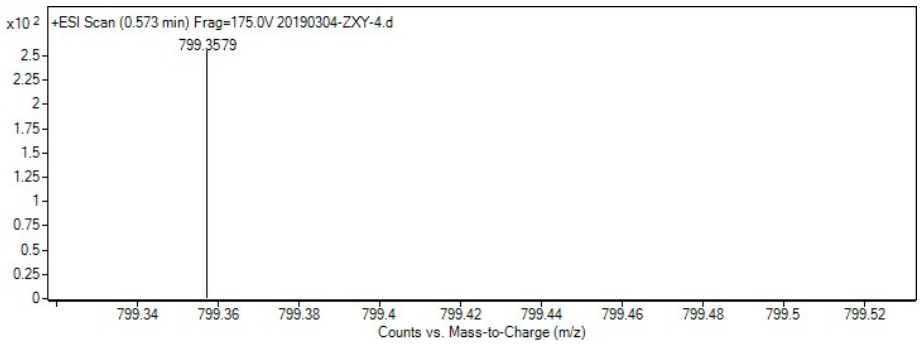

HRMS spectra of compound ***S*-6**

References

1. F. D. Meng, F. Li, L. Yang, Y. X. Wang, Y. W. Quan, Y. X. Cheng., *Polym. Chem*., **2018**, *56*, 1282.
2. X. Yang, X. C. Liu, K. Shen, C. J. Zhu, Y. X. Cheng., *Org. Lett*., **2011**, *13*, 3510.
3. M. Pecul, K. Ruud., *Phys. Chem. Chem. Phys.*, **2011**, *13*, 643.
4. H. R. McAlexander, T. D. Crawford., *J. Chem. Phys.*, **2015**, *142*, 154101.
5. M. J. Frisch, G. W. Trucks, H. B. Schlegel, G. E. Scuseria, M. A. Robb, J. R. Cheeseman, G. Scalmani, V. Barone, B. Mennucci, G. A. Petersson, et al. Gaussian 09, revision D.01; Gaussian, Inc.: Wallingford, CT, **2009.**
6. G. Albano, F. Salerno, L. Portus, W. Porzio, L. A. Aronica, L. D. Bari. *ChemNanoMat*. **2018**, *4*, 1059.